Microresonator-enhanced quantum dot single-photon emission in GaAs-on-insulator platform

Yueguang Zhou, Yuhui Yang, Imad Limame, Priyabrata Mudi, Marcel Hohn, Claudia Piccinini, Battulga Munkhbat, Yann Genuist, Jean-Michel Gerard, Julien Claudon, et al.

Materials for Quantum Technology

PURPOSE-LED PUBLISHING™

ACCEPTED MANUSCRIPT • OPEN ACCESS

Microresonator-enhanced quantum dot single-photon emission in GaAs-on-insulator platform

To cite this article before publication: Yueguang Zhou *et al* 2024 *Mater. Quantum. Technol.* in press https://doi.org/10.1088/2633-4356/ad88cb

Microresonator-enhanced quantum dot single-photon emission in GaAs-on-insulator platform

Yueguang Zhou[1,2,*], Yuhui Yang[2,*], Imad Limame[2], Priyabrata Mudi[2], Marcel Hohn[2], Claudia Piccinini[1], Battulga Munkhbat[1], Yann Genuist[3], Jean-Michel Gérard[4], Julien Claudon[4], Kresten Yvind[1], Niels Gregersen[1], Stephan Reitzenstein[2,*], and Minhao Pu[1,*]

[1]DTU Electro, Department of Electrical and Photonics Engineering, Technical University of Denmark, Ørsteds Plads 343, 2800 Kgs. Lyngby, Denmark
[2]Institute of Solid State Physics, Technische Universität Berlin, 10623 Berlin, Germany
[3]Univ. Grenoble Alpes, CNRS, Grenoble INP, Institut Néel, "Nanophysique et semiconducteurs" group, F-38000 Grenoble, France
[4]Univ. Grenoble Alpes, CEA, Grenoble INP, IRIG, PHELIQS, "Nanophysique et semiconducteurs" group, F-38000 Grenoble, France
[*]These authors contributed equally to this work.

E-mail: ngre@dtu.dk, stephan.reitzenstein@physik.tu-berlin.de, mipu@dtu.dk

Abstract. Single-photon emitters play a crucial role in integrated photonic quantum systems across various material platforms. In this study, we present a cavity-enhanced quantum dot single-photon source in a high-index contrast material platform (GaAs-on-insulator). A quantum dot is embedded in a microring resonator with a quality factor of approximately 9000, where the cavity-induced light enhancement results in a spontaneous emission acceleration factor of around 2.6, and we achieve a $g^{(2)}(0)$ as low as 0.03 ± 0.02 and post-selected two-photon interference visibility of $51.7\% \pm 3.2\%$ for the single-photon source. This demonstration shows the potential of the GaAs-on-Insulator platform for scalable on-chip quantum information processing.

1. Introduction

Quantum information technology has garnered remarkable attention for its potential in unprecedented computation speed and highly secure communication [1, 2]. A critical component in developing quantum computation or communication systems is a single-photon emitter that can deterministically generate indistinguishable photons with high purity on demand [3, 4]. Several candidates exist for deterministic single-photon emitters, such as 2D material-type emitters, color centers in SiC and diamond [5–7].

Among the available choices, III-V quantum dots (QDs) distinguish themselves with their superior attributes, including remarkable brightness and excellent optical and quantum optical emission properties [3, 4, 8]. Notably, they exhibit enhanced thermal stability and photostability in single-photon emission [9–11], compared for example to their colloidal counterparts [12, 13]. Therefore, they are considered prime candidates for implementing photonic quantum information systems [14]. However, QDs in bulk material face challenges in photon extraction efficiency due to the high refractive index environment [15]. Overcoming this challenge requires proper photonic engineering, such as integrating QDs into waveguides or cavities, which has been demonstrated in different material platforms such as suspended GaAs membranes, deep-etching GaAs/AlGaAs platforms, and hybrid material platform [16–18]. The exploration of these integrated material platforms becomes imperative for achieving large-scale quantum information processing. In the case of InAs QDs, the original integrated platform is the native GaAs/AlGaAs layer stack. However, achieving sufficient optical confinement in this material system often necessitates deep etching, resulting in additional optical losses [19, 20]. To address this issue, a suspended GaAs thin film can be patterned by wet etching the underlying AlGaAs layer [21, 22]. This approach ensures a high index contrast between the GaAs membrane and air, reducing the need for deep etching. However, this platform may encounter challenges such as mechanical instability and limited scalability. To solve these issues, hybrid integration techniques can be employed, such as flip-chip bonding or transfer printing, enabling the integration of III-V QDs on lower-index materials like SiO_2 and SiN [18, 23–25]. In this concept, single photons emitted from QDs in the GaAs layer are adiabatically coupled to the SiN waveguide, with SiO_2 serving as an intermediate layer between the two materials. The higher-index contrast of this material system provides benefits such as higher coupling efficiency from the emitter to waveguides, and it avoids the challenging deep etching [18, 26]. To date, SiN quantum circuits have shown low optical losses, as low as 1 dB/m, making them highly promising for large-scale quantum information processing applications [25]. In this work, we demonstrate a new high-index contrast material platform, namely GaAs-on-insulator, for quantum information processing with the light solely propagating in the high-confinement GaAs waveguide. In contrast to integrating QDs onto SiN through evanescent coupling, we opt for the direct embedding of QDs into GaAs waveguides. This approach not only minimizes fabrication complexity but also eliminates coupling losses between different material layers arising from misalignment and fabrication imperfections.

In our experiments, we integrated QDs into a GaAs microring cavity to couple the photons emitted by a selected QD into a microring cavity. Here, by utilizing cavity quantum electrodynamics (cQED) effects in the weak coupling regime, the emission rate of the selected QD into the resonant modes of the ring resonator can be increased via the Purcell effect. Additionally, the Purcell effect improves the single photon coherence, by accelerating spontaneous emission rates with respect to dephasing processes [14, 27, 28]. Compared to other types of optical cavities such as the micropillar cavity and Bullseye

cavity [3], the microring cavity is a planar waveguide cavity, which can be a candidate for the on-chip quantum photonic circuits. In addition, the multiple cavity resonances and small free spectral range can also increase the likelihood of coupling a QD into resonances, which lowers the challenge of spectrally aligning a QD with the cavity resonance. However, the achievable light-matter interaction strength of the microring cavity is compromised by its relatively large mode volume. The fabricated GaAs micro-ring resonator exhibits a quality factor (Q) of approximately 9000, resulting in a spontaneous emission acceleration factor (F) of around 2.6. The coupling efficiency (β) from the QD to the ring modes is estimated to be 62%. Cavity-enhanced emission of a single QD gives rise to single-photon emission with a $g^{(2)}(0)$ of 0.03±0.02 and two-photon interference post-selected visibility of $51.7\% \pm 3.2\%$. Our work introduces a new integrated platform, GaAs-on-insulator (GaAsOI), for quantum information processing, where single-photon sources, and other functional photonic components such as beam splitters, couplers, phase shifters, and detectors can be seamlessly integrated into the same material.

2. GaAs-on-insulator micro-ring resonator fabrication

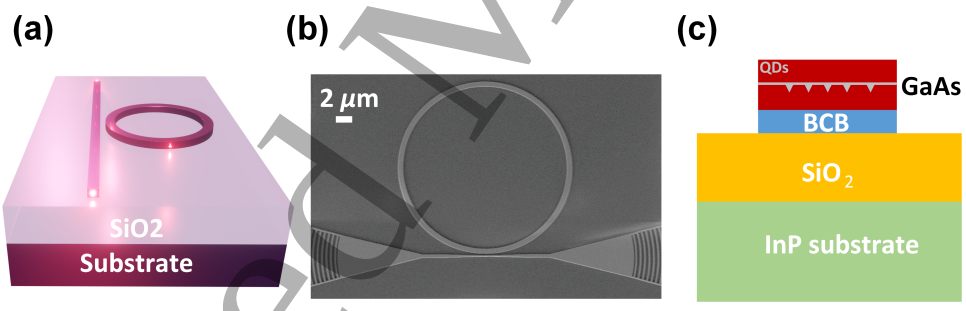

Figure 1. (a) Schematic of micro-ring cavity-based single-photon source in the GaAs-on-insulator platform. The shining cone is depicted as a QD; (b) Scanning electron microscope (SEM) image of the micro-ring cavity. The bar indicates a scale of 2 μm. (c) Layout of the GaAs-on-insulator material platform.

Figure 1(a) illustrates a GaAs micro-ring resonator that incorporates an embedded QD. In this configuration, photons emitted from the QD are initially coupled into the micro-ring resonator and subsequently guided towards an integrated bus waveguide. Finally, the photons are scattered out through two grating out-couplers, as visualized in the scanning electron microscopy (SEM) image shown in Figure 1(b). The ring radius is 10 μm. Regarding the width of the waveguide of the ring cavity, the highest coupling efficiency is achieved for the GaAsOI waveguide with a width of 220 nm and height of 110 nm [26]. However, to mitigate the degradation of the QDs from the surface states in the etched sidewall, a minimal distance of 300 nm is required [29]. On the other hand, the wider the waveguide leads to the lower coupling efficiency. Thus, after weighing both considerations, we have chosen the waveguide width to be 600 nm, leading to a

free spectral range (FSR) of 2.1 nm. Similarly, a thickness of 140 nm of the GaAs layer is chosen as a compromise ensuring reasonable coupling efficiency [26]. The bus waveguide width at the coupling point is 170 nm and the coupling gap between the ring cavity waveguide and bus waveguide is 120 nm. The theoretical Q factor of the microring cavity is around 87,000 as simulated by a commercial Finite Element Method solver (JCMsuite), which only considered the coupling loss from the ring cavity to the bus waveguide. With the assumption that the photon is coupled into two contra-propagating traveling wave modes, the mode volume (V) is approximated as the production of the effective mode area and the circumference of the ring resonator. The effective mode area is derived by a Finite Difference Eigenmode numerical solver (Lumerical, MODE), which is $\sim 0.043(\lambda)^2$. Hereby the mode volume is $\sim 124(\lambda/n)^3$, where n is the refractive index of GaAs (3.47). In the experiments, we collected the single-photon emission on top of the grating couplers, which features a theoretical extraction efficiency for the TE mode of around 60% within a 10° collection angle relative to the vertical axis.

The fabrication process of the GaAsOI device consists of two primary steps. Firstly, the GaAsOI sample is created, followed by the patterning of nanostructures on the GaAs thin film. The original wafer structure comprises a 140 nm thick GaAs thin film containing QDs in the center positioned on top of a 400 nm $Al_{0.8}Ga_{0.2}As$ layer. This layered structure is grown on a GaAs substrate using the molecular beam epitaxy (MBE) method [30]. Subsequently, the original sample is flip-chip bonded to an InP substrate using the methodology outlined in Refs. [31,32]. A two-step etching process is employed to remove the GaAs substrate. Initially, a fast etching step is performed using a mixture of H_2SO_4 and H_2O_2, followed by a slower etching using a mixture of citric acid and H_2O_2. During this process, the 400 nm $Al_{0.8}Ga_{0.2}As$ layer acts as an etch-stop layer, which is subsequently eliminated using a 5% HF solution. To define the microring structure, we spin hydrogen silsesquioxane (HSQ) resist on the GaAsOI sample and pattern it using electron beam lithography (EBL). This process is carried out using a JEOL system (JBX-9500FS) operating at 100 kV. Subsequently, the GaAs layer is etched using a boron trichloride (BCl_3)-based dry etching process in an inductively coupled plasma reactive ion etching (ICP-RIE) machine [33]. The final material layout of the GaAsOI microring, as depicted in Figure 1(c), consists of a 140 nm thick GaAs layer on top of 3 μm thick SiO_2 layer. The intermediate layer, composed of Benzocyclobutene (BCB), has a thickness of approximately 2 μm. Since we aim to demonstrate the functionality of the GaAsOI platform for on-chip quantum circuits, we did not perform deterministic fabrication by imaging the QDs. In our fabrication, an array of microring cavities was patterned on the GaAsOI sample [34]. By analyzing the photoluminescence spectrum, we could determine the QDs coupled into the ring resonance modes.

3. Experiment setup

In our experimental setup, the sample is placed inside a closed-cycle cryostat to maintain low temperatures (4 K). The setup consists of three main paths: the top excitation

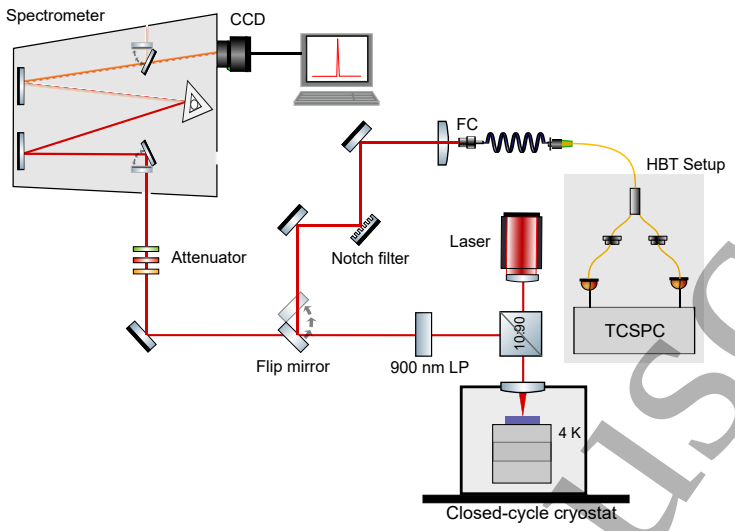

Figure 2. Schematic of the spectroscopic setup with the pump laser at 860 nm. LP: long pass filter; FC: ferrule connector; HBT: Hanbury Brown and Twiss; TCSPC: time-correlated single-photon counter.

path, the collection path for Hanbury Brown and Twiss (HBT) measurements, and the collection path for spectrally resolved micro-photoluminescence (μPL) measurements. In the excitation path, we use a pulse laser (PicoEmerald, APE) to pump the sample at 860 nm with a repetition rate of 80 MHz. During the experiment, we illuminate the QDs within the ring resonator, and the emitted photons are collected on the grating coupler, as depicted in Figure 1(b). The collected photons pass through an aspheric lens (NA = 0.65) and a 900 nm long-pass filter to eliminate the pump light. A flip mirror can switch the two collection paths. In the HBT measurement path, we employ a notch filter as a narrow-band pass filter (spectral width: 0.4±0.1 nm, transmission: 95%), which allows us to isolate the emission line of a single QD. The reflected photons are collected by a single-mode fiber, which is then split into two branches using a fiber-based beamsplitter. These two branches are connected to two superconducting nanowire single-photon detectors (SQ080u2, Single Quantum Eos). The detection events are correlated using a time-correlated single-photon counter (TCSPC, quTAG) to measure the HBT correlations with a temporal resolution of 80 ps. For the μPL spectra measurement path, the photons are reflected by a mirror and measured by a spectrometer.

Figure 3 characterizes the under-study QD coupled into the microresonator resonance with the photon being collected on top of the grating coupler. Figure 3(a) shows excitation power dependence photoluminescence (PL) intensity, which features a saturation power of saturation power (P_{sat}) of 82 μW. Additionally, Figure 3(b) reveals the emission characteristics of QDs with the collection on top of the grating coupler, showcasing a distinct linear polarization. The linear polarization emission can be attributed to the coupling of the QD exclusively with the transverse electric (TE) mode and to the output grating coupler being optimized for this TE mode.

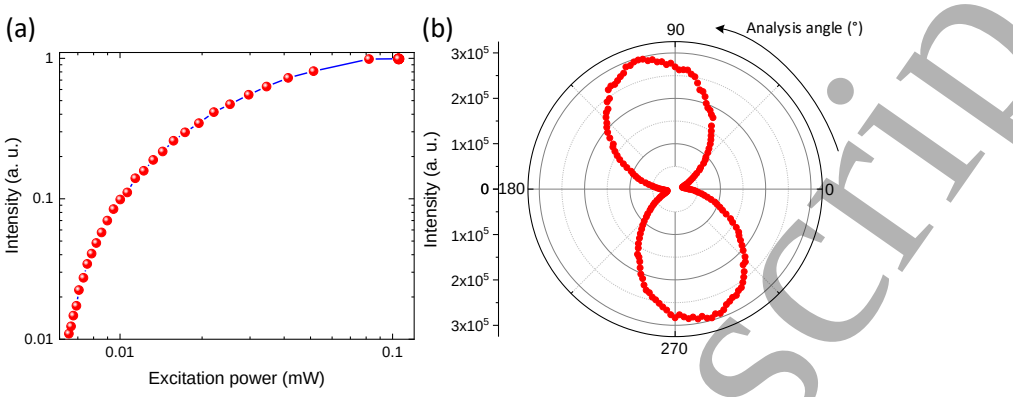

Figure 3. (a) PL intensity as a function of the excitation power for the QD under study. (b) Polarization analysis of the PL.

4. Results and discussion

Coupling the QD to the cavity resonance can enhance both the brightness and the single-photon properties [35]. In our experiment, we exploit the difference in the temperature-dependent spectral shift between the QD emission line and the cavity resonance to control their coupling [36]. Figure 4(a) illustrates the tuning process. As the temperature increases from 4 K to 34 K, the cavity resonance remains relatively stable whereas the QD emission experiences a pronounced redshift. The spectral resonance between the photonic mode and the QD emission is achieved at around 20 K; it is accompanied by strong emission enhancement of the coupled QD-cavity system in the weak coupling regime of cQED. To further illustrate the cavity-enhanced increase of QD emission intensity, Fig. 4(b) showcases a comparison of the PL spectra close to resonance (22 K) and off-resonance (34 K). The PL spectra exhibit an approximate six-fold difference in the intensity of the QD emission. Moreover, the quality factor of the fundamental TE mode cavity resonance is approximately 9000. This value is directly determined by fitting the bare cavity resonance peak at 34 K. The deviation from the theoretical Q factor is attributed to fabrication imperfections and the underestimated absorption coefficient of GaAs at this wavelength. There is another broad emission peak in the range of 908.0 to 908.5 nm, which is likely due to a higher-order transverse mode cavity resonance of the multimode waveguide with a width of 600 nm. We assume that at 34 K this mode is illuminated by other (weakly coupled) QDs in spectral resonance with this mode at this temperature.

In order to further investigate the Purcell enhancement provided by the ring-resonator, we performed time-resolved μPL measurements of the coupled QD-microring system. Figure 5(a) displays the results of these measurements, comparing the QD emission at different temperatures ‡ and off-resonance (at 32 K). The PL decay is well-

‡ The difference between the temperature to reach the best coupling condition compared to Fig.4 might be due to the lagging between the nominal temperature of the heating unit and the QD chip.

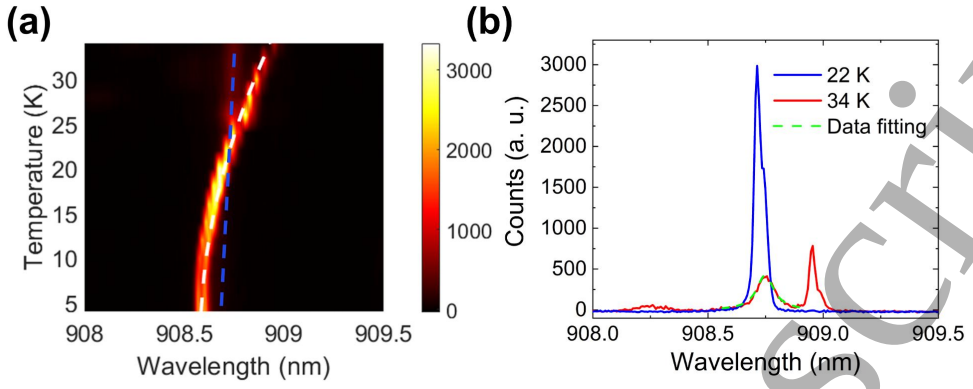

Figure 4. (a) Temperature-dependent photoluminescence map of a coupled QD-microring system. The white and light blue dashed lines indicate the trajectory of the wavelength shift of QD emission and the cavity resonance, respectively. (b) μPL spectra with the QD emission close to resonance (22 K) and off-resonance (34 K) with the microring mode, respectively. The dashed line shows a Lorentzian fitting for the cavity resonance at 34 K, which features a quality factor of around 9000.

described with a double-exponential decay model [37]. At 20 K, the fast decay rate is determined to be around 0.60±0.01 ns, whereas when the QD is tuned off-resonance, it exhibits a decay rate of around 1.55±0.02 ns (32 K). To determine the spontaneous emission acceleration factor, F, Fig. 5(b) illustrates the change in the QD decay time as the QD transition crosses the cavity resonance by changing the temperature. By comparing the decay time at 20 K (on resonance) to the maximum lifetime at 32 K (off-resonance), we can derive a F of approximately 2.6 and a Purcell factor (F_p) of 1.6 with $F_p = F - 1$ [28]. This indicates more than a factor of two-times enhancement of the spontaneous emission rate of the QD due to light-matter interaction in the weak coupling regime when it is resonantly coupled to the optical cavity. Furthermore, the asymmetry in off-resonance decay time at varying temperatures is due to faster QD wavelength shift at higher temperatures [38], leading to an asymmetric QD lifetime with temperature tuning.

When the emitter linewidth is much smaller than the cavity linewidth, the theoretical Purcell factor can be estimated by $F_P = \frac{3}{4\pi^2}\left(\frac{\lambda}{n}\right)^3 \frac{Q}{V}$ [28]. This Purcell factor formula can be applied to our microring cavity since the extracted linewidth of QD from the PL spectra of 34 K in Fig. 4(b) is about 0.03 nm and the linewidth of the cavity resonance is about 0.10 nm, which determines a F_p of ∼5.5 and a F of ∼6.5 with a measured Q of ∼9,000 and a theoretical mode volume of $\sim 124(\lambda/n)^3$, based on the assumption of perfect spatial, spectral and polarization alignment between the cavity resonance and emitter [28]. The discrepancy between the experimental and theoretical spontaneous emission acceleration factor can be due to spatial misalignment between the emitter and the maximum of the waveguide mode electric field profile. This misalignment can be mitigated by introducing a deterministic fabrication technique [34]. In an ideal scenario that the QD has perfect spatial and spectral alignment with the

cavity resonance, β can be approximated by $F_p/(F_p+\gamma)$, where γ is the normalized spontaneous emission rate into the leaky modes, *i.e.*, $\gamma = 1$. It gives the theoretical β of 84%. On the other hand, although the position of the QD with respect to the maximum field intensity position along the radial direction in experiments is unknown, the experimental β from the QD to the ring cavity modes can still be approximated by: $\beta = (F-\gamma)/F$, [39]. With the experimental F of 2.6, β is determined around 62%. The good experimental β can account for the six-times increased intensity observed in Fig. 4(a) when tuning the QD coupled into resonance.

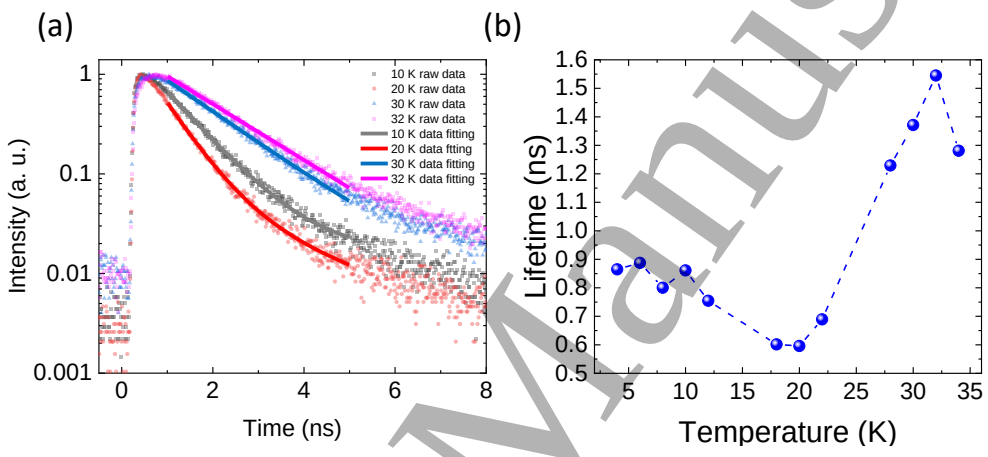

Figure 5. (a) Time-resolved μPL measurements of the QD at different temperature. The decay time is 0.86±0.01 ns (10 K), 0.60±0.01 ns (20 K), 1.37±0.02 ns (30 K), and 1.55±0.02 ns (32 K), respectively. (b) The PL decay time of the QD as a function of temperature.

Furthermore, we investigated the quantum nature of emission by measuring the second-order autocorrelation function ($g^{(2)}(\tau)$) at resonance. The experimental result, depicted in Fig. 6(a), reveals strong photon anti-bunching at a relatively low excitation power of 2 μW (0.02×P_{sat}, normalized to the saturation power of QD, P_{sat}=82 μW). The associated multi-photon suppression is determined by a calculated $g^{(2)}(0)$ value of 0.17, obtained by comparing the integration of the raw data of the central peak within 12.5 ns and its first right neighboring peak in the same range ($g^{(2)}_{raw}(0)$). The non-ideal single-photon purity is due to the dark counts of the system and the background emission from the InP substrate. To account for the influence of uncorrelated background emission, we fit each peak of the raw data with the following expression [22]:

$$g^{(2)}(\tau) = A_0 e^{-|\tau-\tau_0|\gamma} + A_1 \sum_n e^{-|\tau-\tau_0-n\tau_{\rm rep}|\gamma} + c \qquad (1)$$

where A_0 denotes the central peak area, A_1 the side peak areas, γ the decay rate, $\tau_{\rm rep}$ the pulse repetition time, τ_0 the time offset to centralize the function, n the peak numbers, and c the background noise from the environments. By fitting the data, we obtained the value of $g^{(2)}(0)$ as A_0/A_1 ($g^{(2)}_{fit}(0)$), and the fitting error range was derived from the

confidence bounds in the range of 95% of the fitting. For Fig. 6(a), the calculated $g^{(2)}_{fit}(0)$ value is 0.03±0.02, which indicates the excellent single-photon purity of the QD single-photon source. However, as we increased the excitation power to $0.2\times P_{sat}$, a more pronounced peak emerged at the center of the data, resulting in $g^{(2)}_{raw}(0)$=0.35 and $g^{(2)}_{fit}(0)$= 0.10±0.01. Figure 6(c) presents the excitation power dependence of $g^{(2)}(0)$ in detail, which unveils the degradation in single-photon purity at higher excitation power levels. This result indicates a power-dependent increase of uncorrelated background emission of off-resonant emitters due to the off-resonant coupling effect at high excitation power [40], as often observed for cavity-enhanced QD single-photon sources [41]. In addition, the stronger background emission from the InP substrate can also result in degradation, which can be replaced with silicon substrate in the future.

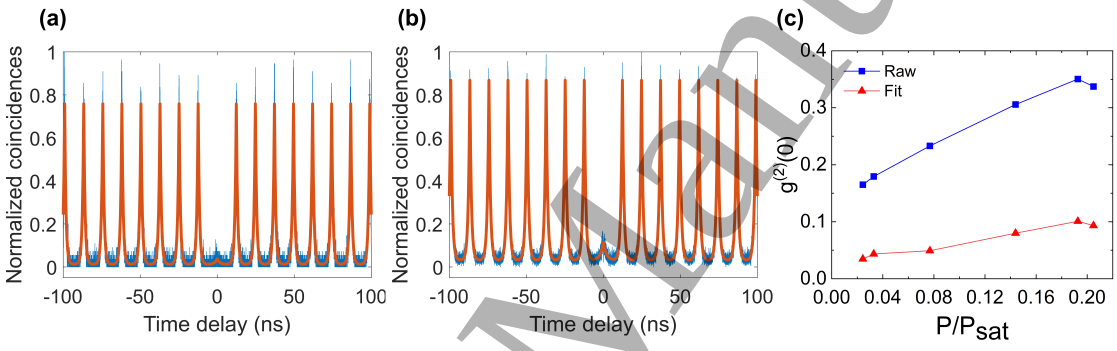

Figure 6. Second-order autocorrelation of the resonantly coupled QD-microring system for different excitation powers (a) 2.0 μW and (b) 16.8 μW. (c) $g^{(2)}(0)$ as a function of excitation power (P) normalized to the P_{sat} of the QD, P_{sat}=82 μW.

In addition to the purity, another important figure of the merit of an SPS is the single-photon indistinguishability. We further measure the Hong-Ou-Mandel (HOM) interference of the QD as shown in Fig. 7 with an excitation power of 70.1 μW. The visibility (V) of the HOM interference is defined as: $V = 1 - \left(A_{\parallel}/A_{\perp}\right)$ with $A_{\parallel}$ and $A_{\perp}$ being the area of the center peak for the measured $g^{(2)}(\tau)$ for parallel polarization and cross polarization. In our HOM setup, the fiber delay is relatively short about 4 ns, which leads to the overlap between neighboring peaks as shown in Fig. 7. The raw visibility (V_{raw}) is merely 11.7%. To get rid of the overlap of the coincidence peaks in the measurements, we fit $g^{(2)}(\tau)$ for the two polarization measurements with the following two expressions:

$$f_{\parallel} = \frac{2}{\pi}\left[A_0\frac{\tau_1^2}{4\left(t-t_0\right)^2+\tau_1^2} + \sum_{i=1}^{3} A_i\frac{\tau_1^2}{4\left(t-t_i\right)^2+\tau_1^2} + \sum_{i=1}^{3} A_i'\frac{\tau_1^2}{4\left(t+t_i\right)^2+\tau_1^2}\right] \quad (2)$$

$$f_{\perp} = \frac{2}{\pi}\left[A_0\frac{\tau_1^2}{4\left(t-t_0\right)^2+\tau_1^2} + \sum_{i=1}^{3} A_i\frac{\tau_1^2}{4\left(t-t_i\right)^2+\tau_1^2} + \sum_{i=1}^{3} A_i'\frac{\tau_1^2}{4\left(t+t_i\right)^2+\tau_1^2}\right] \quad (3)$$

where A_0 is the center peak area, A_i and A_i' are the peak area on the left side and right side, respectively. Here we fit the three peaks on each side and the center peak. We further extract A_0 for the two polarization measurements. We can derive the temporal post-selected visibility V_{fit}=51.7% ± 3.2%. The non-ideal indistinguishability is mainly due to the impure single-photon emission and the dephasing from the environmental fluctuations, for example, charging noise due to the surface states, which can be eliminated by the surface passivation process. In addition, the background emission from the InP substrate can also contaminate the indistinguishability. To further improve the two-photon interference visibility, resonant excitation can be employed, which needs strict suppression of the excitation laser [29, 42]. The excitation laser suppression challenge can be mitigated in our microring system by resonantly pumping the QD within the ring resonator, and then collecting the emitted photon through the grating coupler, while simultaneously operating the excitation laser in a cross-polarized configuration relative to the TE mode polarization due to the weak coupling from the cross-polarized excitation laser into both the waveguide and the grating coupler.

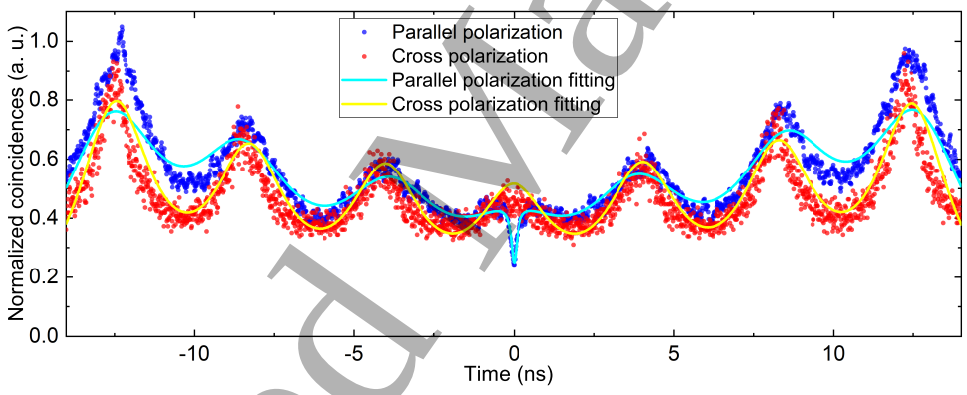

Figure 7. Hong-Ou-Mandel interference experiments under pulsed excitation with 4 ns fiber delay with an excitation power of 70.1 μW.

5. Conclusion

In this study, we demonstrated a cavity-enhanced QD single-photon source on a high-index contrast GaAs-on-Insulator platform compatible with integrated quantum information processing, eliminating the need for suspension and deep etching processes. Our microring cavity exhibited a quality factor of approximately 9000, allowing for a spontaneous emission acceleration factor of approximately 2.6 and a Purcell factor of about 1.6. The coupling efficiency from the QD to the ring cavity modes is estimated to be 62%. Owing to the good optical properties of the resonantly coupled QD-microcavity system, we achieved a $g^{(2)}(0)$ as low as 0.03±0.02 and two-photon interference visibility of 51.7% ± 3.2%, showcasing the platform's capability for generating high-quality single photons into on-chip integrated waveguide circuits. Based on our theoretical calculations, we anticipate that by precisely positioning the QDs, we can enhance the

Purcell factor to 5.5 and increase the coupling efficiency to 84%. This enhancement is expected to further increase the brightness and the visibility of two-photon interference of the QD microring single-photon sources. Overall, our results provide compelling evidence for the functionality of the GaAs-on-insulator platform for on-chip quantum circuits. Furthermore, this platform can accommodate other integrated components such as optical splitters, phase shifters, and superconducting nanowire single photon detectors [43, 44], which opens up the possibilities for implementing comprehensive quantum information processing systems on a single platform.

6. Acknowledgement

This work is funded by the European Union's Horizon 2020 Research and Innovation Programme under the Marie Sklodowska-Curie Grant Agreement No. 861097, by the European Research Council (ERC-StG "REFOCUS" grant 853522, ERC-CoG "UNITY" grant 865230), by the Independent Research Fund. Denmark (Grant No. DFF-9041-00046B) and by the German Research Foundation via projects RE2974/29-1 and INST 131/795-1 FUGG, and the Einstein foundation via the Einstein Research Unit "Perspectives of a quantum digital transformation: Near-term quantum computational devices and quantum processors". The authors would like to appreciate the fruitful discussion with Dr. Pawel Holewa from the Technical University of Denmark and Dr. Liang Zhai from the University of Basel.

7. Reference

[1] O'brien J L, Furusawa A and Vučković J 2009 *Nature Photon.* **3** 687–695
[2] Wang J, Sciarrino F, Laing A and Thompson M G 2020 *Nature Photon.* **14** 273–284
[3] Senellart P, Solomon G and White A 2017 *Nature Nanotechnol.* **12** 1026–1039
[4] Wang H, He Y M, Chung T H, Hu H, Yu Y, Chen S, Ding X, Chen M C, Qin J, Yang X *et al.* 2019 *Nature Photon.* **13** 770–775
[5] He Y M, Clark G, Schaibley J R, He Y, Chen M C, Wei Y J, Ding X, Zhang Q, Yao W, Xu X *et al.* 2015 *Nature Nanotechnol.* **10** 497–502
[6] Castelletto S, Johnson B, Ivády V, Stavrias N, Umeda T, Gali A and Ohshima T 2014 *Nature Materi.* **13** 151–156
[7] Atatüre M, Englund D, Vamivakas N, Lee S Y and Wrachtrup J 2018 *Nature Rev. Materi.* **3** 38–51
[8] Tomm N, Javadi A, Antoniadis N O, Najer D, Löbl M C, Korsch A R, Schott R, Valentin S R, Wieck A D, Ludwig A *et al.* 2021 *Nature Nanotechnol.* **16** 399–403
[9] Holewa P, Burakowski M, Musiał A, Srocka N, Quandt D, Strittmatter A, Rodt S, Reitzenstein S and Sek G 2020 *Sci. Rep.* **10** 21816
[10] Yana Y, Jo B, Kim J, Lee C R, Kim J S, Oh D K, Jong S K and Leem J Y 2009 *J. Appl. Phys.* **105**
[11] Chatzarakis N, Germanis S, Thyris I, Katsidis C, Stavrinidis A, Konstantinidis G, Hatzopoulos Z and Pelekanos N 2023 *Phys. Rev. Appl.* **20** 034011
[12] Ji Y, Wang M, Yang Z, Qiu H, Ji S, Dou J and Gaponenko N V 2020 *Nanoscale* **12** 6403–6410
[13] Bimberg D, Grundmann M and Ledentsov N N 1999 *Quantum dot heterostructures* (John Wiley & Sons)
[14] Heindel T, Kim J H, Gregersen N, Rastelli A and Reitzenstein S 2023 *Adv. Opt. Photonics* **15** 613

[15] Barnes W, Björk G, Gérard J, Jonsson P, Wasey J, Worthing P and Zwiller V 2002 *Eur. Phys. J. D* **18** 197–210

[16] Lodahl P, Mahmoodian S and Stobbe S 2015 *Rev. of Mod. Phys.* **87** 347

[17] Zhang X, Takeuchi K, Cong X, Xiong Y, Morifuji M, Maruta A, Kajii H and Kondow M 2017 *Jpn. J. Appl. Phys.* **56** 126501

[18] Davanco M, Liu J, Sapienza L, Zhang C Z, De Miranda Cardoso J V, Verma V, Mirin R, Nam S W, Liu L and Srinivasan K 2017 *Nature commun.* **8** 889

[19] 2014 *Opt. Commun.* **327** 49–55 special Issue on Nonlinear Quantum Photonics

[20] Volatier M, Duchesne D, Morandotti R, Arès R and Aimez V 2010 *Nanotechnology* **21** 134014

[21] Uppu R, Pedersen F T, Wang Y, Olesen C T, Papon C, Zhou X, Midolo L, Scholz S, Wieck A D, Ludwig A *et al.* 2020 *Sci. Advan.* **6** eabc8268

[22] Kiršanskė G, Thyrrestrup H, Daveau R S, Dreeßen C L, Pregnolato T, Midolo L, Tighineanu P, Javadi A, Stobbe S, Schott R *et al.* 2017 *Phys. Rev. B* **96** 165306

[23] Stepanov P, Delga A, Zang X, Bleuse J, Dupuy E, Peinke E, Lalanne P, Gérard J M and Claudon J 2015 *Appl. Phys. Lett.* **106**

[24] Schnauber P, Singh A, Schall J, Park S I, Song J D, Rodt S, Srinivasan K, Reitzenstein S and Davanco M 2019 *Nano Lett.* **19** 7164–7172

[25] Chanana A, Larocque H, Moreira R, Carolan J, Guha B, Melo E G, Anant V, Song J, Englund D, Blumenthal D J *et al.* 2022 *Nature Commun.* **13** 7693

[26] Wang Y, Vannucci L, Burger S and Gregersen N 2022 *Mater. Quantum Technol.* **2** 045004

[27] Gregersen N, McCutcheon D P and Mørk J 2017 *Handbook of Optoelectronic Device Modeling and Simulation* 585–608

[28] Gérard J M 2003 *Top. Appl. Phys.* **90** 269

[29] Liu J, Konthasinghe K, Davanço M, Lawall J, Anant V, Verma V, Mirin R, Nam S W, Song J D, Ma B *et al.* 2018 *Phys, Rev. Appl.* **9** 064019

[30] Gérard J M, Genin J, Lefebvre J, Moison J, Lebouché N and Barthe F 1995 *J. Cryst. Growth.* **150** 351–356

[31] Pu M, Ottaviano L, Semenova E and Yvind K 2016 *Optica* **3** 823–826

[32] Ottaviano L, Pu M, Semenova E and Yvind K 2016 *Opt. Lett.* **41** 3996–3999

[33] Kim C, Ye C, Zheng Y, Semenova E, Yvind K and Pu M 2022 *IEEE. J. Sel. Top. Quantum Electron.* **29** 1–14

[34] Madigawa A A, Donges J N, Gaál B, Li S, Jacobsen M A, Liu H, Dai D, Su X, Shang X, Ni H *et al.* 2023 *ACS Photon.*

[35] Li S, Chen Y, Shang X, Yu Y, Yang J, Huang J, Su X, Shen J, Sun B, Ni H *et al.* 2020 *Nanoscale Res. Lett.* **15** 1–7

[36] Reithmaier J P, Sek G, Löffler A, Hofmann C, Kuhn S, Reitzenstein S, Keldysh L V, Kulakovskii V D, Reinecke T L and Forchel A 2004 *Nature* **432** 197–200 URL `https://doi.org/10.1038/nature02969`

[37] Brooks A, Chu X L, Liu Z, Schott R, Ludwig A, Wieck A D, Midolo L, Lodahl P and Rotenberg N 2021 *Nano Lett.* **21** 8707–8714

[38] Chen J, Markus A, Fiore A, Oesterle U, Stanley R, Carlin J, Houdre R, Ilegems M, Lazzarini L, Nasi L *et al.* 2002 *J. Appl. Phys.* **91** 6710–6716

[39] Moreau E, Robert I, Gérard J, Abram I, Manin L and Thierry-Mieg V 2001 *Appl. Phys. Lett.* **79** 2865–2867

[40] Florian M, Gartner P, Gies C and Jahnke F 2013 *New J. Phys.* **15** 035019

[41] Strauf S, Stoltz N G, Rakher M T, Coldren L A, Petroff P M and Bouwmeester D 2007 *Nature Photon.* **1** 704–708

[42] Lüker S and Reiter D E 2019 *Semicond. Sci. Technol.* **34** 063002

[43] Dietrich C P, Fiore A, Thompson M G, Kamp M and Höfling S 2016 *Laser & Photon. Rev.* **10** 870–894

[44] Wang J, Santamato A, Jiang P, Bonneau D, Engin E, Silverstone J W, Lermer M, Beetz J, Kamp

M, Höfling S *et al.* 2014 *Opt. Commun.* **327** 49–55